

# An Asymptotically Optimal Approximation of the Conditional Mean Channel Estimator based on Gaussian Mixture Models

Michael Koller, Benedikt Fesl, Nurettin Turan, and Wolfgang Utschick, *Fellow, IEEE*

**Abstract**—This paper investigates a channel estimator based on Gaussian mixture models (GMMs) in the context of linear inverse problems with additive Gaussian noise. We fit a GMM to given channel samples to obtain an analytic probability density function (PDF) which approximates the true channel PDF. Then, a conditional mean estimator (CME) corresponding to this approximating PDF is computed in closed form and used as an approximation of the optimal CME based on the true channel PDF. This optimal CME cannot be calculated analytically because the true channel PDF is generally unknown. We present mild conditions which allow us to prove the convergence of the GMM-based CME to the optimal CME as the number of GMM components is increased. Additionally, we investigate the estimator's computational complexity and present simplifications based on common model-based insights. Further, we study the estimator's behavior in numerical experiments including multiple-input multiple-output (MIMO) and wideband systems.

**Index Terms**—asymptotic convergence, conditional mean channel estimation, Gaussian mixture models, machine learning, spatial channel model

## I. INTRODUCTION

Channel estimation plays a critical role in future mobile communications systems, e.g., [2]–[4]. The mean square error (MSE) minimizing channel estimator is known as conditional mean estimator (CME). Computing the CME in closed form requires analytic knowledge of the channel probability density function (PDF). Even if the PDF was known, calculating the CME might not be possible analytically or not be tractable practically. Increasingly, advanced channel models (e.g., [5]) or simulators (e.g., [6]–[8]) are used to generate large amounts of realistic channel samples. In a real application, channel samples can, for example, be collected at the base station to be used in addition to or instead of the simulated data. Importantly, such data represent the whole scenario (or environment) in which the base station is placed. It is thus interesting to investigate data-based algorithms to design channel estimators which are applicable to a whole scenario.

The following approach is taken in this paper. First, channel samples are used to fit a Gaussian mixture model (GMM). Since GMMs can approximate any continuous PDF [9],

the fitted GMM is a PDF which approximates the unknown true channel PDF. Second, given the GMM PDF, the corresponding CME can be expressed in closed form. Thanks to the approximation by Gaussian mixtures, the closed-form CME is a weighted sum of linear minimum mean square error (LMMSE) filters which use the first-order and second-order moments of the GMM components. Due to the preparatory offline fitting process, no covariance estimation is necessary when the LMMSE filters are applied for (online) channel estimation. Since the GMM PDF approximates the true channel PDF, we ask whether the GMM-based CME approximates the true CME.

A related work is [10], where the authors assume that the channel is GMM-distributed and study the available closed-form CME for example in the asymptotic high signal-to-noise ratio (SNR) regime to derive pilot signals. In this work, we do not assume that the channel is GMM-distributed. Instead, a GMM is used as an approximation of the true channel PDF and we analyze whether the corresponding CME is an approximation of the true CME. This can be viewed as a study of the GMM estimator in the high number of GMM components regime. A main contribution of this paper is to prove that as the number of components increases, the GMM CME converges to the optimal CME if the observation matrix is invertible (cf. Theorem 2). For noninvertible observation matrices, we make a weaker statement. Moreover, we analyze the GMM estimator's computational complexity and show how the complexity can be reduced in different estimation scenarios. This is also demonstrated in numerical simulations.

We study the GMM estimator in numerical simulations where we consider both multiple-input multiple-output (MIMO) and wideband channel estimation scenarios with both invertible and noninvertible observation matrices. The considered channel data come from a 3GPP channel model [5] and from the QuaDRiGa channel simulator [6], [7] so that they are not GMM-distributed by construction. The generated data represent a scenario where for example a base station covers a certain sector with users whose positions are drawn uniformly at random. The obtained GMM estimator is then suited for channel estimation in the whole scenario.

The paper is structured as follows. Section II introduces the signal model discussed throughout the paper as well as particular instances thereof which are used in numerical simulations. Section III reviews GMMs and channel estimation literature which employs them. The main part is Section IV where we

This work was supported by the Deutsche Forschungsgemeinschaft under grant UT 36/21.

Preliminary results have been submitted to ICASSP'22, cf. preprint [1].  
The authors are with Professur für Methoden der Signalverarbeitung, Technische Universität München, 80333 München, Germany, e-mail: {michael.koller,benedikt.fesl,nurettin.turan,utschick}@tum.de

investigate the GMM-based CME and study its convergence to the optimal CME as well as its computational complexity. Sections V and VI present state-of-the-art channel estimation algorithms, channel models, and numerical simulations.

*Notation:* The supremum norm of a continuous function  $f : \mathbb{R}^N \rightarrow \mathbb{R}$  is given by  $\|f\|_\infty = \sup_{\mathbf{x} \in \mathbb{R}^N} |f(\mathbf{x})|$ , and  $\|\mathbf{x}\|$  is the Euclidean norm of  $\mathbf{x} \in \mathbb{C}^N$ . A real- or complex-valued normal distribution with mean vector  $\boldsymbol{\mu}$  and covariance matrix  $\mathbf{C}$  is denoted by  $\mathcal{N}(\boldsymbol{\mu}, \mathbf{C})$  or  $\mathcal{N}_{\mathbb{C}}(\boldsymbol{\mu}, \mathbf{C})$ , respectively. The vectorization (stacking columns) of a matrix  $\mathbf{X} \in \mathbb{C}^{m \times N}$  is written as  $\text{vec}(\mathbf{X}) \in \mathbb{C}^{mN}$ , and  $\mathbf{A} \otimes \mathbf{B} \in \mathbb{C}^{m_1 m_2 \times N_1 N_2}$  is the Kronecker product of  $\mathbf{A} \in \mathbb{C}^{m_1 \times N_1}$  and  $\mathbf{B} \in \mathbb{C}^{m_2 \times N_2}$ .

## II. SIGNAL MODELS

We consider the generic signal model

$$\mathbf{y} = \mathbf{A}\mathbf{h} + \mathbf{n}, \quad \mathbf{n} \sim \mathcal{N}_{\mathbb{C}}(\mathbf{0}, \boldsymbol{\Sigma}) \quad (1)$$

where  $\mathbf{h} \in \mathbb{C}^N$  is the channel,  $\mathbf{A} \in \mathbb{C}^{m \times N}$  is the observation matrix, and  $\mathbf{n} \in \mathbb{C}^m$  is additive white Gaussian noise. The observation  $\mathbf{y} \in \mathbb{C}^m$ , the matrix  $\mathbf{A}$ , the noise mean vector  $\mathbf{0} \in \mathbb{C}^m$ , and the noise covariance matrix  $\boldsymbol{\Sigma} \in \mathbb{C}^{m \times m}$  are given. The goal of channel estimation is to recover  $\mathbf{h}$  from (1).

In this paper, we study a channel estimation algorithm which is designed using the given signal model as well as a data set of channel samples. While the main part addresses the generic signal model (1), we consider the following three instances of it in numerical simulations.

### A. Single-Input Multiple-Output Signal Model

The single-input multiple-output (SIMO) signal model is for instance appropriate if a single-antenna mobile device transmits pilot signals to a base station with  $N$  antennas which receives

$$\mathbf{y} = \mathbf{h} + \mathbf{n} \in \mathbb{C}^N. \quad (2)$$

This model is interesting for us because the observation matrix is the identity matrix and therefore invertible. Further, the performance of the proposed channel estimator can be studied without having to take into account the difficulty of choosing a suitable observation matrix.

### B. Multiple-Input Multiple-Output Signal Model

If a mobile user with  $N_{\text{tx}}$  antennas transmits  $N_p$  pilots to a base station with  $N_{\text{rx}}$  antennas, the receive signal  $\mathbf{Y} \in \mathbb{C}^{N_{\text{rx}} \times N_p}$  can be written as

$$\mathbf{Y} = \mathbf{H}\mathbf{P} + \mathbf{N} \quad (3)$$

where  $\mathbf{H} \in \mathbb{C}^{N_{\text{rx}} \times N_{\text{tx}}}$  is the channel,  $\mathbf{P} \in \mathbb{C}^{N_{\text{tx}} \times N_p}$  is the pilot, and  $\mathbf{N} \in \mathbb{C}^{N_{\text{rx}} \times N_p}$  is the noise matrix. With the definitions  $\mathbf{h} = \text{vec}(\mathbf{H})$ ,  $\mathbf{y} = \text{vec}(\mathbf{Y})$ ,  $\mathbf{n} = \text{vec}(\mathbf{N})$ , and  $\mathbf{A} = \mathbf{P}^T \otimes \mathbf{I}_{N_{\text{rx}}}$ , the MIMO signal model (3) is an instance of (1).

### C. Wideband Signal Model

If we consider a single-input single-output (SISO) transmission in the spatial domain over a frequency-selective fading channel,  $\mathbf{H} \in \mathbb{C}^{N_c \times N_t}$  represents the time-frequency response of the channel for  $N_c$  subcarriers and  $N_t$  time slots. When only  $N_p$  positions of the time-frequency response are occupied with pilot symbols, then there is a *selection matrix*  $\mathbf{A} \in \{0, 1\}^{N_p \times N_c N_t}$  which represents the pilot positions. This leads to the observations as described in (1) with  $\mathbf{h} = \text{vec}(\mathbf{H}) \in \mathbb{C}^{N_c N_t}$ . Regarding the structure of the pilot positions, three different arrangements are commonly considered: block-, comb-, and lattice-type, cf. [11].

## III. GAUSSIAN MIXTURE MODELS IN THE LITERATURE

In this section, we briefly explain GMMs and summarize channel estimation literature which makes use of GMMs.

### A. Gaussian Mixture Models

A GMM with  $K$  components is a PDF of the form [12]

$$f_{\mathbf{h}}^{(K)}(\mathbf{h}) = \sum_{k=1}^K p(k) \mathcal{N}_{\mathbb{C}}(\mathbf{h}; \boldsymbol{\mu}_k, \mathbf{C}_k) \quad (4)$$

consisting of a weighted sum of  $K$  Gaussian PDFs. The probabilities  $p(k)$  are called *mixing coefficients*, and  $\boldsymbol{\mu}_k \in \mathbb{C}^N$  and  $\mathbf{C}_k \in \mathbb{C}^{N \times N}$  denote the mean vector and covariance matrix of the  $k$ th GMM component, respectively. As explained in [12], GMMs allow to calculate the *responsibilities*  $p(k | \mathbf{h})$  by evaluating Gaussian likelihoods:

$$p(k | \mathbf{h}) = \frac{p(k) \mathcal{N}_{\mathbb{C}}(\mathbf{h}; \boldsymbol{\mu}_k, \mathbf{C}_k)}{\sum_{i=1}^K p(i) \mathcal{N}_{\mathbb{C}}(\mathbf{h}; \boldsymbol{\mu}_i, \mathbf{C}_i)}. \quad (5)$$

This is an important property for our considerations.

Given data samples, an expectation-maximization (EM) algorithm can be used to fit a  $K$ -components GMM [12]. The data-based fitting process determines the mixing coefficients, the mean vectors, and the covariance matrices. A detailed introduction to GMMs and the corresponding well-known EM algorithm can, e.g., be found in [12].

### B. Gaussian Mixture Models in Channel Estimation Literature

In [13], channels are modeled as sparse vectors whose non-zero coefficients are GMM-distributed. A combination of EM and approximate message passing (AMP) is then introduced for channel estimation. The algorithm simultaneously estimates the GMM parameters. Building on this work, [14] model the beam domain channels via GMMs in the context of uplink channel estimation with pilot contamination. The authors of [15] then investigate the approach further including a new initialization technique for the algorithm. In [16], the beam domain channel is also assumed to be GMM-distributed and a modification of learned AMP is proposed for sparse channel estimation.

The authors of [17] model temporal channel variations as GMMs, e.g., in order to predict channel states. The authors of [18] propose to improve channel estimation techniques by using GMMs as a better characterization of the noise in a

communications environments than it is given by the additive white Gaussian noise model. In [19], a GMM prior is used for the unknown data symbols in semi-blind channel estimation.

GMMs are also employed for channel clustering tasks. For example, [20] use GMMs for channel multipath clustering. In [21], a *power weighted GMM* is proposed to increase the clustering performance. Another variation of GMMs, called *rotationally invariant GMM*, can be found in [22].

In [10], [23], the true channel PDF is assumed to be equal to a GMM and the authors then investigate the corresponding CME to optimize the pilot matrix. To this end, the asymptotic high-SNR regime of the CME is studied. Further, an information-theoretic criterion for pilot optimization is introduced because the MSE of the estimator has no closed-form expression and is thus not suitable as optimization criterion [10].

In this paper, we study the same GMM-based estimator as the authors of [10], [23]. However, we do not assume that the true channel PDF is equal to a GMM. Instead, we take the GMM as an approximation of the true channel PDF and we ask whether the corresponding GMM-based estimator is then an approximation of the true CME (based on the true channel PDF). In this sense, we study the GMM-based estimator's behavior in the high number of components regime and our work complements [10] by motivating the application of the estimator in a wider class of channel models.

#### IV. MAIN PART

The MSE-optimal channel estimate for the model (1) is given by the conditional expectation  $E[\mathbf{h} | \mathbf{y}]$ , cf., e.g., [24]. However, the true channel PDF is generally not known and, therefore,  $E[\mathbf{h} | \mathbf{y}]$  can generally not be calculated analytically. Even if the true channel PDF was known, the CME  $E[\mathbf{h} | \mathbf{y}]$  might still not have an analytic expression. In this section, we investigate a GMM-based CME with closed-form expression and prove that it converges to the optimal CME as the number of GMM components is increased. Further, we discuss its computational complexity and how the complexity can be reduced.

##### A. Channel Estimator

GMMs are known to be able to approximate any continuous PDF arbitrarily well [9]. In particular, if  $f_{\mathbf{h}}$  denotes the PDF of the channel which is assumed to be continuous, then there exists a sequence  $(f_{\mathbf{h}}^{(K)})_{K=1}^{\infty}$  of GMMs which converges uniformly to  $f_{\mathbf{h}}$ . To define a GMM-based estimator, let  $f_{\mathbf{n}}$  and  $f_{\mathbf{y}}$  be the PDFs of the noise and the observation, respectively, and let us first observe the following:

$$f_{\mathbf{h}|\mathbf{y}}(\mathbf{h} | \mathbf{y}) = \frac{f_{\mathbf{y}|\mathbf{h}}(\mathbf{y} | \mathbf{h})f_{\mathbf{h}}(\mathbf{h})}{f_{\mathbf{y}}(\mathbf{y})} = \frac{f_{\mathbf{n}}(\mathbf{y} - \mathbf{A}\mathbf{h})f_{\mathbf{h}}(\mathbf{h})}{f_{\mathbf{y}}(\mathbf{y})}. \quad (6)$$

With this the optimal CME can be expressed as

$$\hat{\mathbf{h}} = E[\mathbf{h} | \mathbf{y}] = \int \mathbf{h} \frac{f_{\mathbf{n}}(\mathbf{y} - \mathbf{A}\mathbf{h})f_{\mathbf{h}}(\mathbf{h})}{f_{\mathbf{y}}(\mathbf{y})} d\mathbf{h}. \quad (7)$$

For every  $K \in \mathbb{N}$ , we now consider the model

$$\mathbf{y}^{(K)} = \mathbf{A}\mathbf{h}^{(K)} + \mathbf{n} \quad (8)$$

where  $\mathbf{h}^{(K)}$  is distributed according to the GMM  $f_{\mathbf{h}}^{(K)}$  which has the form (4). Since we have a sequence  $(f_{\mathbf{h}}^{(K)})_{K=1}^{\infty}$  of GMMs, the parameters  $p(k)$ ,  $\boldsymbol{\mu}_k$ , and  $\mathbf{C}_k$  would also depend on the sequence index  $K$  but we omit it for readability. Let  $f_{\mathbf{y}}^{(K)}$  be the PDF of  $\mathbf{y}^{(K)}$ . We now define a GMM-based estimator

$$\hat{\mathbf{h}}^{(K)} := E^{(K)}[\mathbf{h}^{(K)} | \mathbf{y}] := \int \mathbf{h} \frac{f_{\mathbf{n}}(\mathbf{y} - \mathbf{A}\mathbf{h})f_{\mathbf{h}}^{(K)}(\mathbf{h})}{f_{\mathbf{y}}^{(K)}(\mathbf{y})} d\mathbf{h} \quad (9)$$

by replacing  $f_{\mathbf{h}}$  and  $f_{\mathbf{y}}$  in (7) with  $f_{\mathbf{h}}^{(K)}$  and  $f_{\mathbf{y}}^{(K)}$ , respectively, because similar to (6) we have

$$f_{\mathbf{h}|\mathbf{y}}^{(K)}(\mathbf{h} | \mathbf{y}) = \frac{f_{\mathbf{n}}(\mathbf{y} - \mathbf{A}\mathbf{h})f_{\mathbf{h}}^{(K)}(\mathbf{h})}{f_{\mathbf{y}}^{(K)}(\mathbf{y})}. \quad (10)$$

The law of total expectation allows us to write

$$\hat{\mathbf{h}}^{(K)} = \sum_{k=1}^K p(k | \mathbf{y}) E^{(K)}[\mathbf{h}^{(K)} | \mathbf{y}, k] \quad (11)$$

in order to introduce the GMM mixing variable. Since  $\mathbf{h}^{(K)} | k$  is Gaussian, also  $\mathbf{A}\mathbf{h}^{(K)} | k$  and therefore  $\mathbf{y}^{(K)} | k$  are Gaussian. The mean vector and covariance matrix of  $\mathbf{y}^{(K)} | k$  are  $E[\mathbf{y}^{(K)} | k] = \mathbf{A}\boldsymbol{\mu}_k$  and

$$E[(\mathbf{y}^{(K)} - \mathbf{A}\boldsymbol{\mu}_k)(\mathbf{y}^{(K)} - \mathbf{A}\boldsymbol{\mu}_k)^H | k] = \mathbf{A}\mathbf{C}_k\mathbf{A}^H + \boldsymbol{\Sigma}, \quad (12)$$

respectively. The well-known LMMSE formula can now be used to compute

$$E^{(K)}[\mathbf{h}^{(K)} | \mathbf{y}, k] = \mathbf{C}_k\mathbf{A}^H(\mathbf{A}\mathbf{C}_k\mathbf{A}^H + \boldsymbol{\Sigma})^{-1}(\mathbf{y} - \mathbf{A}\boldsymbol{\mu}_k) + \boldsymbol{\mu}_k \quad (13)$$

which can be plugged into (11).

In order to calculate  $p(k | \mathbf{y})$  in (11), we compute the PDF

$$f_{\mathbf{y}}^{(K)}(\mathbf{y}) = \sum_{k=1}^K p(k) \mathcal{N}_{\mathbb{C}}(\mathbf{y}; \mathbf{A}\boldsymbol{\mu}_k, \mathbf{A}\mathbf{C}_k\mathbf{A}^H + \boldsymbol{\Sigma}), \quad (14)$$

which is a GMM. GMMs allow to calculate the responsibilities by evaluating Gaussian likelihoods (cf. Section III-A):

$$p(k | \mathbf{y}) = \frac{p(k) \mathcal{N}_{\mathbb{C}}(\mathbf{y}; \mathbf{A}\boldsymbol{\mu}_k, \mathbf{A}\mathbf{C}_k\mathbf{A}^H + \boldsymbol{\Sigma})}{\sum_{i=1}^K p(i) \mathcal{N}_{\mathbb{C}}(\mathbf{y}; \mathbf{A}\boldsymbol{\mu}_i, \mathbf{A}\mathbf{C}_i\mathbf{A}^H + \boldsymbol{\Sigma})}. \quad (15)$$

Plugging this into (11) shows that as soon as the mixing coefficients  $p(k)$  as well as the means  $\boldsymbol{\mu}_k$  and covariances  $\mathbf{C}_k$  are given, the estimator  $\hat{\mathbf{h}}^{(K)}$  can be computed in closed form by combining (11), (13), and (15), which results in (16). As discussed next in Section IV-B, various quantities of the GMM estimator can be precomputed at this point to save computational complexity: the products involving the known observation matrix  $\mathbf{A}$  and means  $\boldsymbol{\mu}_k$  and covariance matrices  $\mathbf{C}_k$  as well as the LMMSE filters including the computationally costly matrix inverse in (16). To obtain the GMM parameters, the channel PDF  $f_{\mathbf{h}}$  needs to be approximated by fitting a  $K$ -components GMM to given channel samples, cf. Section III-A.

A possible application scenario of the GMM estimator would be to use channel samples collected at, for example, the base station of a cellular radio system to construct a site-specific GMM channel estimator. In an initial (offline) training

phase, the channel samples are used to fit a  $K$ -components GMM. Afterwards, (online) channel estimates are computed via (16).

### B. Computational Complexity

To compute  $\hat{\mathbf{h}}^{(K)}$  in (16),  $K$  responsibilities  $p(k | \mathbf{y})$  (15) and  $K$  LMMSE formulas (13) need to be evaluated. Since both the matrix  $\mathbf{A}$  and the GMM covariance matrices  $\mathbf{C}_k$  do not change between observations, the inverse in (13) can be precomputed offline for various SNRs. Thus, evaluating (13) online is dominated by matrix-vector multiplications and has a complexity of  $\mathcal{O}(N^2)$  for  $m \leq N$ . The responsibilities are calculated by evaluating Gaussian densities, as can be seen from (15). A Gaussian density with mean  $\boldsymbol{\mu} \in \mathbb{C}^N$  and covariance matrix  $\mathbf{C} \in \mathbb{C}^{N \times N}$  can be written as

$$\mathcal{N}_{\mathbb{C}}(\mathbf{x}; \boldsymbol{\mu}, \mathbf{C}) = \frac{\exp(-(\mathbf{x} - \boldsymbol{\mu})^H \mathbf{C}^{-1} (\mathbf{x} - \boldsymbol{\mu}))}{\pi^n \det(\mathbf{C})}. \quad (17)$$

Again, since the GMM covariance matrices and mean vectors do not change between observations, the inverse and the determinant of the densities in (15) can be precomputed offline. Thus, the online evaluation is again dominated by matrix-vector multiplications and has a complexity of  $\mathcal{O}(N^2)$ . The resulting overall complexity of computing  $\hat{\mathbf{h}}^{(K)}$  is  $\mathcal{O}(KN^2)$ .

In some cases, as demonstrated in the following subsections, the computational complexity can be reduced by constraining the GMM covariance matrices  $\mathbf{C}_k$  such that corresponding matrix-vector multiplications are accelerated. In other cases, the number of GMM parameters might be reduced by introducing covariance matrix constraints which can enhance the convergence of the EM algorithm, improve the resulting estimation performance, and reduce the required amount of channel samples. Particular choices for constraints can come from scenario-specific insights. We demonstrate the feasibility of the following two constraint examples in Section VI.

1) *Circulant covariance matrices:* A first example is a scenario, where the base station employs a uniform linear array (ULA) and where the channel covariance matrix therefore is Toeplitz structured. For large numbers of antennas, a Toeplitz matrix is well approximated by a circulant matrix [25]. Any circulant matrix  $\mathbf{C} \in \mathbb{C}^{N \times N}$  has an eigendecomposition of the form  $\mathbf{C} = \mathbf{F} \text{diag}(\mathbf{c}) \mathbf{F}^H$  where  $\mathbf{F} \in \mathbb{C}^{N \times N}$  is the discrete Fourier transform (DFT) matrix and where  $\mathbf{c} \in \mathbb{C}^N$ . Consequently, thanks to fast Fourier transforms, matrix-vector multiplications involving circulant matrices can be performed in  $\mathcal{O}(N \log(N))$  time. For a large number of antennas, we therefore have a motivation to use circulant covariance matrices  $\mathbf{C}_k = \mathbf{F} \text{diag}(\mathbf{c}_k) \mathbf{F}^H$  in the GMM.

This is particularly interesting for a signal model where  $\mathbf{A} = \mathbf{I}$  and  $\boldsymbol{\Sigma} = \sigma^2 \mathbf{I} = \sigma^2 \mathbf{F} \mathbf{F}^H$ . In this case, the LMMSE formula (13) simplifies to

$$\mathbf{E}[\mathbf{h} | \mathbf{y}, k] = \mathbf{F} \text{diag}(\mathbf{d}_k) \mathbf{F}^H (\mathbf{y} - \boldsymbol{\mu}_k) + \boldsymbol{\mu}_k \quad (18)$$

where the  $i$ th entry of the vector  $\mathbf{d}_k$  is given by  $[\mathbf{d}_k]_i = \frac{[\mathbf{c}_k]_i}{[\mathbf{c}_k]_i + \sigma^2}$ , such that (18) can be calculated in  $\mathcal{O}(N \log(N))$  time. With a circulant  $\mathbf{C} = \mathbf{F} \text{diag}(\mathbf{c}) \mathbf{F}^H$ , (17) reads as

$$\mathcal{N}_{\mathbb{C}}(\mathbf{x}; \boldsymbol{\mu}, \mathbf{F} \text{diag}(\mathbf{c}) \mathbf{F}^H) = \frac{\exp(-(\mathbf{F}(\mathbf{x} - \boldsymbol{\mu}))^H \text{diag}(\mathbf{c})^{-1} \mathbf{F}(\mathbf{x} - \boldsymbol{\mu}))}{\pi^n \prod_{i=1}^N [\mathbf{c}]_i}. \quad (19)$$

A first observation is that this can also be evaluated in  $\mathcal{O}(N \log(N))$  time such that computing channel estimates  $\hat{\mathbf{h}}^{(K)}$  has a complexity of  $\mathcal{O}(KN \log(N))$  if circulant covariance matrices are used in the GMM. A second observation is that the Gaussian density (19) has a significantly reduced number of parameters:  $N + N$  (mean vector  $\boldsymbol{\mu}$  and covariance vector  $\mathbf{c}$ ) in contrast to  $N + \frac{N(N+1)}{2}$  (mean vector  $\boldsymbol{\mu}$  and covariance matrix  $\mathbf{C}$ ) in (17). This simplifies the EM algorithm iterations of the GMM fitting process and reduces the number of required training channel samples. For this latter reason, even if  $\mathbf{A} \neq \mathbf{I}$ , one might be interested in employing a GMM with circulant covariance matrices. The relationship between the number of channel samples and the EM algorithm's performance is demonstrated in Section VI. In an implementation, instead of constraining the covariance matrices to be circulant, all channel samples can be Fourier transformed as  $\tilde{\mathbf{h}} = \mathbf{F} \mathbf{h}$  and then the GMM's covariance matrices can be constrained to be diagonal matrices due to the relation  $\mathbf{C} = \mathbf{F} \text{diag}(\mathbf{c}) \mathbf{F}^H$ .

2) *Kronecker covariance matrices:* Another example where complexity can be reduced is the MIMO signal model from Section II-B. A well-known assumption for spatial correlation scenarios is that the scattering in the vicinity of the transmitter and of the receiver are independent of each other, cf. [26]. In this case, every channel covariance matrix  $\mathbf{C}$  can be decomposed into the Kronecker product of a transmit and receive side spatial covariance matrix:  $\mathbf{C} = \mathbf{C}_{\text{tx}} \otimes \mathbf{C}_{\text{rx}}$ . Here, we have a motivation to use a GMM with Kronecker product covariance matrices  $\mathbf{C}_k = \mathbf{C}_{\text{tx},k} \otimes \mathbf{C}_{\text{rx},k}$ .

To this end, instead of fitting a single GMM using the vectorized channel data of dimension  $N = N_{\text{tx}} N_{\text{rx}}$ , one can fit two independent transmit and receive side GMMs of dimensions  $N_{\text{tx}}$  and  $N_{\text{rx}}$ , respectively. This not only results in lower offline training complexity and in the ability to parallelize, but also in a smaller number of training channel samples needed because the respective GMMs have much fewer parameters. The training channel samples for these low-dimensional GMMs are obtained by taking the rows (columns) of the available channel matrices independently in order to fit the transmit (receive) side GMM. In order to then obtain the full-size covariance matrices  $\mathbf{C}_k$ , all combinatorial Kronecker products of transmit and receive side covariance matrices  $\mathbf{C}_{\text{tx},i}$  and  $\mathbf{C}_{\text{rx},j}$  are computed. The details are described in the numerical simulations section.

In this example, plugging the Kronecker decomposition  $\mathbf{C}_k = \mathbf{C}_{\text{tx},k} \otimes \mathbf{C}_{\text{rx},k}$  into the LMMSE formula (13) does not lead to an expression that simplifies to a Kronecker product. This is because the inverse in (13) can generally not be written in terms of a Kronecker product and, thus, full matrix-vector products are necessary. However, [27] explains how (13) can be approximated by means of a Kronecker product in the

$$\hat{\mathbf{h}}^{(K)} = \sum_{k=1}^K \frac{p(k)\mathcal{N}_{\mathbb{C}}(\mathbf{y}; \mathbf{A}\boldsymbol{\mu}_k, \mathbf{A}\mathbf{C}_k\mathbf{A}^H + \boldsymbol{\Sigma})}{\sum_{i=1}^K p(i)\mathcal{N}_{\mathbb{C}}(\mathbf{y}; \mathbf{A}\boldsymbol{\mu}_i, \mathbf{A}\mathbf{C}_i\mathbf{A}^H + \boldsymbol{\Sigma})} (\mathbf{C}_k\mathbf{A}^H(\mathbf{A}\mathbf{C}_k\mathbf{A}^H + \boldsymbol{\Sigma})^{-1}(\mathbf{y} - \mathbf{A}\boldsymbol{\mu}_k) + \boldsymbol{\mu}_k) \quad (16)$$

described setting, which might be interesting if computational complexity of (13) is an issue. Nonetheless, even if the online computational complexity is not affected, Kronecker GMM covariance matrices can still be beneficial, for instance, if the number of available channel samples is small. We demonstrate this case in the numerical simulations section.

### C. Convergence of the Estimator

This subsection uses a universal approximation result of [9] to show that if  $f_{\mathbf{h}}$  is continuous, then the GMM-based estimator  $\hat{\mathbf{h}}^{(K)}$  in (9) can approximate the optimal CME  $\hat{\mathbf{h}}$  in (7) arbitrarily well as the number  $K$  of GMM components is increased. The intuition is that if a sequence of PDFs  $f_{\mathbf{h}}^{(K)}$ , which is used in (9), converges to the channel PDF  $f_{\mathbf{h}}$ , we can conjecture that also  $f_{\mathbf{y}}^{(K)}$  from (14) converges to  $f_{\mathbf{y}}$  and that then  $\hat{\mathbf{h}}^{(K)}$  in (9) converges to the optimal CME  $\hat{\mathbf{h}}$  in (7).

Recall that the PDF of a complex random vector can be expressed by means of a joint PDF of its real and imaginary parts. Therefore, this subsection considers real-valued quantities only and the results generalize to the complex-valued setting by considering stacked real and imaginary parts.

To state the main result, we adopt some definitions from [9]. Let  $\mathcal{C} = \{f : \mathbb{R}^N \rightarrow \mathbb{R} : f \geq 0, \int f(\mathbf{x})d\mathbf{x} = 1, f \text{ continuous}\}$  denote the set of all continuous PDFs. Further, let  $g$  denote the standard Gaussian density and define the class of  $K$ -component location-scale finite Gaussian mixtures as

$$\mathcal{M}_K = \left\{ h : h(\mathbf{x}) = \sum_{k=1}^K c_k \frac{1}{\sigma_k^N} g\left(\frac{\mathbf{x} - \boldsymbol{\mu}_k}{\sigma_k}\right) \right\} \quad (20)$$

with

$$\boldsymbol{\mu}_k \in \mathbb{R}^N, \sigma_k > 0, c_k \geq 0 \quad \text{for all } k \in \{1, \dots, K\}, \quad (21)$$

and  $\sum_{k=1}^K c_k = 1$ . Then, any continuous PDF can be approximated arbitrarily well by means of GMMs, as (one part of) [9, Theorem 5] states:

**Theorem 1.** *Let  $\mathcal{C}_0 = \{f \in \mathcal{C} : \forall \varepsilon > 0, \exists \text{ a compact } \mathcal{K} \subset \mathbb{R}^N \text{ such that } \sup_{\mathbf{x} \in \mathbb{R}^N \setminus \mathcal{K}} |f(\mathbf{x})| < \varepsilon\}$  denote the set of all continuous PDFs which vanish at infinity. For any  $f \in \mathcal{C}_0$ , there exists a sequence  $(f^{(K)})_{K=1}^{\infty}$  with  $f^{(K)} \in \mathcal{M}_K$  with*

$$\lim_{K \rightarrow \infty} \|f - f^{(K)}\|_{\infty} = 0. \quad (22)$$

Note that since a PDF is integrable, it always vanishes at infinity such that this is not a constraint for our considerations. As mentioned, we now work with real quantities  $\mathbf{y} = \mathbf{A}\mathbf{h} + \mathbf{n}$  where  $\mathbf{n}$  is a real Gaussian random vector with mean zero and covariance matrix  $\boldsymbol{\Sigma} \in \mathbb{R}^{N \times N}$  whose PDF we denote by  $f_{\mathbf{n}} \in \mathcal{C}_0$ . The PDF of  $\mathbf{h}$  is  $f_{\mathbf{h}}$  and the PDF of  $\mathbf{y}$  is  $f_{\mathbf{y}}$ . The following theorem is proved in Appendix A.

**Theorem 2.** *With the notation defined above, let  $\mathbf{A} \in \mathbb{R}^{N \times N}$  be invertible and let  $f_{\mathbf{h}} \in \mathcal{C}_0$  be arbitrary. Let  $(f_{\mathbf{h}}^{(K)})_{K=1}^{\infty}$  be*

*a sequence of PDFs in  $\mathcal{C}_0$  which converges uniformly to  $f_{\mathbf{h}}$ . Then, the estimator*

$$\hat{\mathbf{h}}^{(K)} = \mathbb{E}^{(K)}[\mathbf{h}^{(K)} | \mathbf{y}] = \int \mathbf{h} \frac{f_{\mathbf{n}}(\mathbf{y} - \mathbf{A}\mathbf{h})f_{\mathbf{h}}^{(K)}(\mathbf{h})}{f_{\mathbf{y}}^{(K)}(\mathbf{y})} d\mathbf{h} \quad (23)$$

*approximates the CME*

$$\hat{\mathbf{h}} = \mathbb{E}[\mathbf{h} | \mathbf{y}] = \int \mathbf{h} \frac{f_{\mathbf{n}}(\mathbf{y} - \mathbf{A}\mathbf{h})f_{\mathbf{h}}(\mathbf{h})}{f_{\mathbf{y}}(\mathbf{y})} d\mathbf{h} \quad (24)$$

*in the sense that for any radius  $r > 0$ ,*

$$\lim_{K \rightarrow \infty} \|\hat{\mathbf{h}} - \hat{\mathbf{h}}^{(K)}\| = 0 \quad (25)$$

*holds uniformly for all  $\mathbf{y}$  in the ball  $\mathcal{B}_r = \{\mathbf{y} \in \mathbb{R}^n : \|\mathbf{y}\| \leq r\}$ . Thus, in particular, by finding a suitable  $r > 0$ , (25) can be seen to hold for any given  $\mathbf{y} \in \mathbb{R}^N$ .*

### D. Discussion of Theorem 2

We start with a comment on the implications of the fact that (25) holds uniformly for all  $\mathbf{y}$  in a ball  $\mathcal{B}_r$ . Let  $\mathcal{B}_r$  be given. If we want the error  $\|\hat{\mathbf{h}} - \hat{\mathbf{h}}^{(K)}\|$  to be smaller than a given threshold  $\varepsilon_{\text{thr}} > 0$ , then according to Theorem 2, we can find a  $K_r \in \mathbb{N}$  such that  $\|\hat{\mathbf{h}} - \hat{\mathbf{h}}^{(K)}\| \leq \varepsilon_{\text{thr}}$  holds for all  $\mathbf{y} \in \mathcal{B}_r$  and  $K \geq K_r$ . This does not mean that the error is always larger than  $\varepsilon_{\text{thr}}$  for  $\mathbf{y} \notin \mathcal{B}_r$ . However, it can be the case, that for certain  $\mathbf{y} \notin \mathcal{B}_r$  the number of components  $K$  needs to be strictly larger than  $K_r$  in order for  $\|\hat{\mathbf{h}} - \hat{\mathbf{h}}^{(K)}\|$  to fall below the threshold.

A requirement of Theorem 2 is a sequence of PDFs which converges uniformly to  $f_{\mathbf{h}}$ . By Theorem 1, such a sequence always exists if we consider GMMs. However, as argued in [9], there exist other mixtures with universal approximation properties as well. It is an interesting question whether (9) can be computed in closed form for other mixture models and to see if they for example need fewer components for a satisfying approximation and channel estimation.

Theorem 2 requires  $\mathbf{A}$  to be invertible. Unfortunately, the proof of Theorem 2 cannot be conducted as presented if  $\mathbf{A}$  is not invertible, which is for example the case when we consider a wide matrix with more columns than rows. There are multiple challenges involved. First, the proof makes use of Lemma 1 which shows that  $\int \|\mathbf{h}\| f_{\mathbf{n}}(\mathbf{y} - \mathbf{A}\mathbf{h}) d\mathbf{h}$  is finite for any  $\mathbf{y}$ . This integral is generally not finite if  $\mathbf{A}$  is not invertible (see Appendix B). Second, for invertible  $\mathbf{A}$ , we could directly show that the sequence of PDFs corresponding to  $\mathbf{A}\mathbf{h}^{(K)}$  converges uniformly to the PDF of  $\mathbf{A}\mathbf{h}$ . This will likely not hold for noninvertible  $\mathbf{A}$  (see Appendix C).

While a strong statement about the convergence of the estimators does not seem possible with the presented means if  $\mathbf{A}$  is not invertible, we can make the following observation. Since  $f_{\mathbf{h}}^{(K)}$  converges uniformly to  $f_{\mathbf{h}}$ , it converges in particular pointwise. By Scheffe's lemma (e.g., [28]), it follows that

the random vectors  $\mathbf{h}^{(K)}$  converge to  $\mathbf{h}$  in distribution. We also have  $(\mathbf{h}^{(K)}, \mathbf{n}) \rightarrow (\mathbf{h}, \mathbf{n})$  in distribution. If we define the continuous mapping

$$s: \mathbb{R}^{N+m} \rightarrow \mathbb{R}^{N+m}, (\mathbf{h}, \mathbf{n}) \mapsto (\mathbf{h}, \mathbf{A}\mathbf{h} + \mathbf{n}) \quad (26)$$

then, the continuous mapping theorem (e.g., [29]) implies the convergence of  $s(\mathbf{h}^{(K)}, \mathbf{n}) = (\mathbf{h}^{(K)}, \mathbf{y}^{(K)})$  to  $s(\mathbf{h}, \mathbf{n}) = (\mathbf{h}, \mathbf{y})$  in distribution. Given the convergence in distribution of a sequence  $(\mathbf{h}^{(K)}, \mathbf{y}^{(K)})$  to  $(\mathbf{h}, \mathbf{y})$ , the author of [30] investigates conditions which ensure the convergence of the corresponding conditional expectations  $E[\mathbf{h}^{(K)} | \mathbf{y}^{(K)}]$  to  $E[\mathbf{h} | \mathbf{y}]$ . The main result depends without limitation on the distribution of  $f_{\mathbf{h}}$  which is not assumed to be known in our setting. Reciting the main result is beyond the scope of the current paper and we refer the interested reader to [30].

## V. CHANNEL MODELS AND RELATED CHANNEL ESTIMATORS

Before we turn to numerical simulations, we introduce the considered channel models and discuss other channel estimation algorithms which we use for comparison. At this point, it should be noted that the proposed approach does not rely on estimating a (link-based) covariance matrix based on pilot symbols. Therefore, we do not show comparisons with such approaches as this lies in a different field of applications. To generate channel samples (for training and testing purposes), we define a scenario like for example a base station which covers a certain  $120^\circ$  sector. Afterwards, we choose user positions uniformly at random within the scenario and retrieve their corresponding channels. The so-obtained set of channel samples can then be used to find estimators for the whole scenario. These estimators (both the GMM estimator as well as all estimators introduced in the following) are trained/computed/defined once and then tested on the whole scenario without further modification.

### A. Channel Models

1) *3GPP*: We work with a spatial channel model [5], [31] where channels are modeled conditionally Gaussian:  $\mathbf{h} | \delta \sim \mathcal{N}(\mathbf{0}, \mathbf{C}_\delta)$ . The random vector  $\delta$  collects the angles of arrival/departure and path gains of the main propagation clusters between a mobile terminal and the base station. The main angles are drawn independently and uniformly from the interval  $[0, 2\pi]$  and the path gains are independent zero-mean Gaussians. The base station employs a ULA for both the transmitter and the receiver such that the transmit- and receive-side spatial channel covariance matrix can be computed as

$$\mathbf{C}_\delta^{\{\text{rx}, \text{tx}\}} = \int_{-\pi}^{\pi} g^{\{\text{rx}, \text{tx}\}}(\theta; \delta) \mathbf{a}^{\{\text{rx}, \text{tx}\}}(\theta) \mathbf{a}^{\{\text{rx}, \text{tx}\}}(\theta)^H d\theta. \quad (27)$$

Here,

$$\mathbf{a}^{\{\text{rx}, \text{tx}\}}(\theta) = [1, e^{j\pi \sin(\theta)}, \dots, e^{j\pi(N_{\{\text{rx}, \text{tx}\}}-1)\sin(\theta)}]^T \quad (28)$$

is the array steering vector for an angle of arrival/departure  $\theta$  and  $g$  is a power density consisting of a sum of weighted Laplace densities whose standard deviations describe the angle spread of the propagation clusters [5]. The full channel

covariance matrix is constructed as  $\mathbf{C}_\delta = \mathbf{C}_\delta^{\text{tx}} \otimes \mathbf{C}_\delta^{\text{rx}}$  due to the assumption of independent scattering in the vicinity of transmitter and receiver, see, e.g., [26]. In the SIMO case,  $\mathbf{C}_\delta$  degenerates to the receive-side covariance matrix  $\mathbf{C}_\delta^{\text{rx}}$ . For every channel sample, we generate random angles and path gains, combined in  $\delta$ , and then draw the sample as  $\mathbf{h} \sim \mathcal{N}(\mathbf{0}, \mathbf{C}_\delta)$ .

2) *QuaDRiGa*: Version 2.4 of the QuaDRiGa channel simulator [6], [7] is used to generate channel samples. We simulate an urban macrocell scenario at a center frequency of 2.53 GHz. The base station's height is 25 meters and it covers a  $120^\circ$  sector. The minimum and maximum distances between the mobile terminals and the base station are 35 meters and 500 meters, respectively. In 80% of the cases, the mobile terminals are located indoors at different floor levels, whereas the mobile terminals' height is 1.5 meters in the case of outdoor locations.

QuaDRiGa models the channel of the  $c$ -th carrier and  $t$ -th time symbol as  $\mathbf{H}_{c,t} = \sum_{\ell=1}^L \mathbf{G}_\ell e^{-2\pi j f_c \tau_{\ell,t}}$  where  $\ell$  is the path number, and the number of multi-path components  $L$  depends on whether there is line of sight (LOS), non-line of sight (NLOS), or outdoor-to-indoor (O2I) propagation:  $L_{\text{LOS}} = 37$ ,  $L_{\text{NLOS}} = 61$  or  $L_{\text{O2I}} = 37$ , cf. [32]. The frequency of the  $c$ -th carrier is denoted by  $f_c$  and the  $\ell$ -th path delay of the  $t$ -th time symbol by  $\tau_{\ell,t}$ . The coefficients matrix  $\mathbf{G}_\ell$  consists of one complex entry for each antenna pair, which comprises the attenuation of a path, the antenna radiation pattern weighting, and the polarization [32]. As described in the QuaDRiGa manual [7], the generated channels are post-processed to remove the path gain.

For the simulations in Section VI-A and Section VI-B, we generate single-carrier SIMO and MIMO channels, respectively. The base station is equipped with a ULA with  $N_{\text{rx}}$  "3GPP-3D" antennas and the mobile terminals employ  $N_{\text{tx}}$  "omni-directional" antennas. For the simulations in Section VI-C, we consider a SISO system in the spatial domain with  $N_c$  carriers over a bandwidth of 360 kHz and for a time slot with 1 ms duration that is divided into  $N_t$  time symbols. Each user moves with a certain velocity  $v$  in a random direction.

### B. State-of-the-Art Channel Estimators

A simple baseline algorithm is the least squares (LS) channel estimator which computes

$$\hat{\mathbf{h}}_{\text{LS}} = \mathbf{A}^\dagger \mathbf{y} \quad (29)$$

using the Moore-Penrose pseudoinverse  $\mathbf{A}^\dagger$ . Another immediate estimator consists of first estimating a sample covariance matrix  $\mathbf{C} = \frac{1}{M} \sum_{m=1}^M \mathbf{h}_m \mathbf{h}_m^H$  using  $M = 10^5$  training channel samples drawn uniformly from the whole scenario and then computing LMMSE channel estimates:

$$\hat{\mathbf{h}}_{\text{sample cov.}} = \mathbf{C} \mathbf{A}^H (\mathbf{A} \mathbf{C} \mathbf{A}^H + \mathbf{\Sigma})^{-1} \mathbf{y}. \quad (30)$$

When we work with the 3GPP channel model from Section V-A1, then the true covariance matrix  $\mathbf{C}_\delta$  for every channel sample is available and we can compute a genie LMMSE channel estimate:

$$\hat{\mathbf{h}}_{\text{gen. LMMSE}} = E[\mathbf{h} | \mathbf{y}, \delta] = \mathbf{C}_\delta \mathbf{A}^H (\mathbf{A} \mathbf{C}_\delta \mathbf{A}^H + \mathbf{\Sigma})^{-1} \mathbf{y} \quad (31)$$

which presents a lower bound for all estimators. Note that this is not the optimal CME considered in (7) because of the additional genie knowledge of  $\delta$ .

Compressive sensing approaches assume the channel to be (approximately) sparse:  $\mathbf{h} \approx \mathbf{D}\mathbf{s}$ . Here,  $\mathbf{D} \in \mathbb{C}^{N \times L}$  is a *dictionary* and  $\mathbf{s} \in \mathbb{C}^L$  is a sparse vector. A typical choice for  $\mathbf{D}$  is an oversampled DFT matrix (e.g., [33]). Compressive sensing algorithms then assume that  $\mathbf{y} = \mathbf{A}\mathbf{D}\mathbf{s} + \mathbf{n}$  holds and they recover an estimate  $\hat{\mathbf{s}}$  of  $\mathbf{s}$  and estimate the channel as  $\hat{\mathbf{h}} = \mathbf{D}\hat{\mathbf{s}}$ . A well-known compressive sensing algorithm is orthogonal matching pursuit (OMP) [34]–[36]. OMP needs to know the sparsity order. Since order estimation is a difficult problem, we avoid it via a genie-aided approach: OMP gets access to the true channel to choose the optimal sparsity order. This yields a performance bound for OMP. Another algorithm, which we use for comparison, is AMP [37], [38], which does not need to know the sparsity order.

A convolutional neural network (CNN)-based channel estimator was derived in [31] for the SIMO signal model (cf. Section II-A). In [39], the CNN estimator has been generalized to the MIMO signal model (cf. Section II-B). In the SIMO case, we use the CNN estimator as described in [31]. The activation function is the rectified linear unit and we use the input transform based on the  $2N \times 2N$  Fourier matrix, cf. [31, Equation (43)]. In the MIMO case, we use the CNN estimator as described in [39] where again the activation function is the rectified linear unit. In all cases, the CNN is trained on samples corresponding to the channel model on which it is tested later.

The concept of a concrete autoencoder (CAE) was introduced in [40] and adapted for wideband channel estimation (cf. Section II-C) in [41]. The CAE is an autoencoder where the encoder is replaced by a *concrete selection layer* that selects the  $N_p \ll N_c N_t$  most informative features of the  $N_c N_t$ -dimensional input. This corresponds to designing the pilot matrix by selecting the  $N_p$  pilot positions. The decoder can then be used to perform channel estimation. During training, noisy channels are given as input, such that the decoder of the CAE performs denoising and reconstruction of the full-dimensional channels. Hence, a new CAE needs to be trained for every different SNR. In our simulations, in contrast to [41], no further denoising networks are applied after the CAE.

The authors in [42] propose a deep CNN approach for 2D wideband channel estimation. The estimator, called *Channel-Net*, consists of a combination of an image super-resolution and an image restoration network. Thus, the networks perform interpolation and denoising of the low-dimensional observations with respect to the high-dimensional channel matrix. The super-resolution network consists of three 2D convolution layers, whereas the image restoration network consists of 20 2D convolution layers. Here, too, we train SNR-specific networks.

## VI. NUMERICAL SIMULATIONS

In all simulations, a normalized MSE (nMSE) is used as performance measure. Specifically, we generate  $T = 10^4$   $N$ -dimensional test channel samples  $\{\mathbf{h}_t\}_{t=1}^T$ , obtain corresponding channel estimates  $\hat{\mathbf{h}}_t$ , and define  $\text{nMSE} = \frac{1}{NT} \sum_{t=1}^T \|\mathbf{h}_t - \hat{\mathbf{h}}_t\|^2$ . The noise covariance matrix is  $\Sigma = \sigma^2 \mathbf{I}$ . The test samples are normalized such that  $\mathbb{E}[\|\mathbf{h}\|^2] = N$  holds which allows us to define an SNR as  $\frac{1}{\sigma^2}$ . For training purposes, we generate  $M = 10^5$  channel samples unless stated otherwise. The number of training samples is always chosen large enough such that increasing  $M$  does not lead to a performance improvement during the testing phase. The generated channel samples stem from one of the scenarios described in Section V.

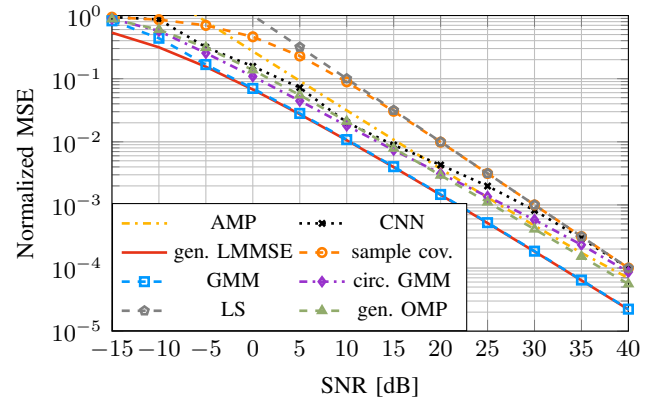


Fig. 1. SIMO signal model (Section II-A) and 3GPP channel model (Section V-A1) with **one** propagation cluster and  $N = 128$  antennas. The performance of the circulant GMM estimator (“circ. GMM”,  $-\cdot-\cdot-$ , Section IV-B1) is shown too. In both cases,  $K = 128$  components are used.

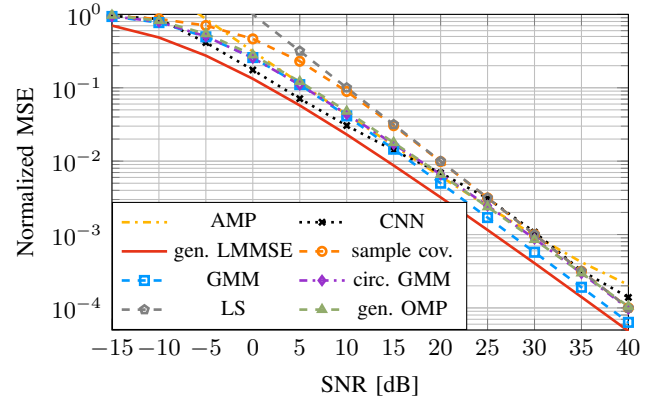


Fig. 2. SIMO signal model (Section II-A) and 3GPP channel model (Section V-A1) with **three** propagation clusters and  $N = 128$  antennas. The performance of the circulant GMM estimator (“circ. GMM”,  $-\cdot-\cdot-$ , Section IV-B1) is shown too. In both cases,  $K = 128$  components are used.

$\hat{\mathbf{h}}_t\|^2$ . The noise covariance matrix is  $\Sigma = \sigma^2 \mathbf{I}$ . The test samples are normalized such that  $\mathbb{E}[\|\mathbf{h}\|^2] = N$  holds which allows us to define an SNR as  $\frac{1}{\sigma^2}$ . For training purposes, we generate  $M = 10^5$  channel samples unless stated otherwise. The number of training samples is always chosen large enough such that increasing  $M$  does not lead to a performance improvement during the testing phase. The generated channel samples stem from one of the scenarios described in Section V.

As explained in Section IV-A, to obtain the GMM-based estimator, we fit one GMM using the available training data via an EM algorithm. Afterwards, inverses which appear in (16) are precomputed for every SNR. In contrast to this approach, the introduced neural network-based estimators need to be newly trained for every SNR at which we evaluate them. This includes searching for suitable hyperparameters for every SNR.

### A. SIMO

Figs. 1 to 4 show channel estimation results for the SIMO signal model from Section II-A. The compressive sensing algorithms OMP and AMP are used with oversampled DFT



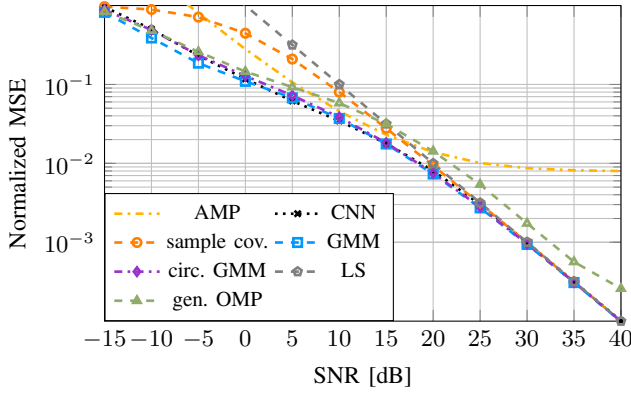


Fig. 3. SISO signal model (Section II-A) and QuaDRiGa channel model (Section V-A2) with  $N = 128$  antennas. The performance of the circulant GMM estimator (“circ. GMM”,  $\text{---}\blacklozenge\text{---}$ , Section IV-B1) is shown too. In both cases,  $K = 128$  components are used.

dictionaries that have  $L = 4N$  and  $L = 2N$  columns, respectively, because these parameters yielded the best results. The number of antennas is always  $N = 128$ . Unless stated otherwise, the GMM fitting process uses  $19 \cdot 10^4$  training data.

In Fig. 1, we consider the 3GPP channel model from Section V-A1 with one propagation cluster. It is interesting to see that the GMM-based estimator performs almost as well as the genie LMMSE estimator. In the mid-SNR range, the two compressive sensing algorithms are approximately equally good. In Fig. 2, we have three propagation clusters. A first observation is the strong performance of the CNN estimator in the mid-SNR range. Note that we can generally not expect any estimator to reach the genie LMMSE curve because it has more channel knowledge (the true covariance matrix for every sample). In the higher SNR-range, the GMM-based estimator is the only algorithm still outperforming LS estimation.

In Fig. 3, we concentrate on the QuaDRiGa channel model described in Section V-A2 where the channel covariance matrices and therefore the genie LMMSE curve are no longer available. Here, the two compressive sensing algorithms behave not as similarly as they did in the previous experiments. Additionally, their performance is not as convincing. A reason might be that the channels now are not sparse enough. The CNN estimator shows again a good performance and overall the GMM-based estimator can compete with it or is better.

In addition to the GMM estimator (16), Figs. 1 to 3 display the performance of the reduced-complexity GMM estimator which uses circulant covariance matrices as described in Section IV-B1. As expected, the estimator’s performance suffers but it is still comparable to the other algorithms. Fig. 3 is particularly interesting where there is not much difference between the full- and low-complexity GMM estimators.

Lastly, Fig. 4 shows the behavior of the GMM-based estimator for different numbers of components,  $K$ . We consider an SNR of 10 dB and the same situation as in Fig. 2: The 3GPP channel model (cf. Section V-A1) with three propagation clusters and  $N = 128$  antennas. In addition to  $K$ , also the number of training data used to fit the GMM is varied. Since the number of parameters of a GMM increases when  $K$  is increased, more training data is necessary for a good fit. This

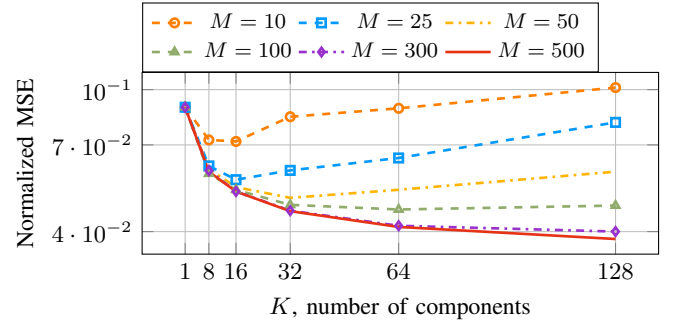


Fig. 4. SISO signal model (Section II-A) and 3GPP channel model (Section V-A1) with **three** propagation clusters and  $N = 128$  antennas. The SNR is 10 dB. The GMM estimator is trained using  $M \cdot 10^3$  samples.

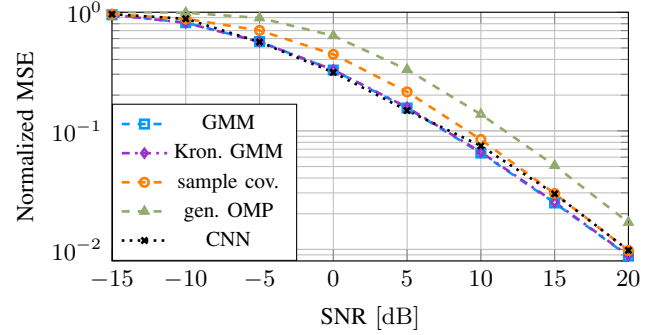


Fig. 5. MIMO signal model (Section II-B) and QuaDRiGa channel model (Section V-A2) with  $(N_{\text{rx}}, N_{\text{tx}}) = (32, 4)$ . The GMM estimator (“GMM”,  $\text{---}\blacksquare\text{---}$ ) uses  $K = 32$  components and the Kronecker GMM estimator (“Kron. GMM”,  $\text{---}\blacklozenge\text{---}$ , Section IV-B2) uses  $K = 4 \times 8$  components.

effect is clearly visible in Fig. 4. Overall, as long as the number of training data is high enough ( $M \geq 300$  in the figure), increasing  $K$  leads to an MSE improvement, which is in accordance with Theorem 2.

Note that we cannot expect the GMM estimator to converge to the genie LMMSE estimator (31) (which is displayed in Fig. 2). The genie LMMSE estimator has more knowledge (namely the true channel covariance matrix  $\mathbf{C}_\delta$ ) and is therefore not the CME,  $\hat{\mathbf{h}} = \mathbb{E}[\mathbf{h} \mid \mathbf{y}]$ , which we want to approximate in Theorem 2. The CME cannot be computed in closed form in the considered scenario which is the main motivation to study the GMM estimator in the first place.

## B. MIMO

For the MIMO simulations whose signal model is described in Section II-B, we use a scaled DFT pilot matrix  $\mathbf{P}$ . Here, we are mainly interested in comparing the GMM estimator in (16) to a GMM estimator which uses Kronecker product covariance matrices as described in Section IV-B2. We generate  $M = 10^5$  training channel samples  $\{\mathbf{H}_i\}_{i=1}^M$  and use them in two different ways. Either, we use the (vectorized) channel matrices  $\mathbf{H}_i$  directly to fit a single  $K = 32$  components GMM. Or, we view all columns and all rows of the data as separate data sets and fit two GMMs: One transmit side GMM with  $K_{\text{tx}} = 4$  components using the rows, one receive side GMM with  $K_{\text{rx}} = 8$  components using the columns. Afterwards, we



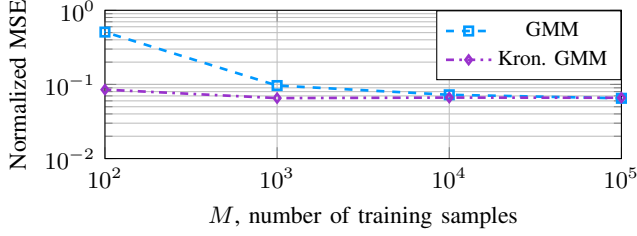


Fig. 6. MIMO signal model (Section II-B) and QuaDRiGa channel model (Section V-A2) with  $(N_{\text{rx}}, N_{\text{tx}}) = (32, 4)$ . The SNR is 10 dB. The Kronecker product GMM estimator (“Kron. GMM”,  $\text{---}\diamond\text{---}$ , Section IV-B2) has fewer parameters than the normal GMM estimator. Both have  $K = 32$  components.

combine the two GMMs to a single full-size GMM with  $K = K_{\text{tx}}K_{\text{rx}} = 32$  components for the whole data set of channel matrices. To this end, the  $K$  full-size means and covariances are directly calculated by combinatorial computation of the Kronecker products of the transmit- and receive-side GMM components. The corresponding mixing coefficients can be computed by fixing the means and covariances and performing a single E-step (cf. [12]) in the EM algorithm to obtain them.

Fig. 5 displays simulation results. A first observation is that the two GMM estimators as well as the CNN estimator perform very similarly, with minor differences in the lower and higher SNR-regimes. Further, these three estimators outperform the sample covariance matrix-based estimator and the genie-aided OMP algorithm, which uses a Kronecker product of two two-times oversampled DFT matrices as dictionary. A second observation is that there is almost no difference between the GMM estimator with or without Kronecker product covariance matrices. This is insofar surprising as the normal GMM consists of  $K = 32$  covariance matrices of dimension  $N \times N$  with  $N = 32 \cdot 4 = 128$  which means that it has  $K \frac{N(N+1)}{2} = 264192$  covariance parameters, whereas in contrast, the Kronecker GMM has only  $K_{\text{rx}} \frac{N_{\text{rx}}(N_{\text{rx}}+1)}{2} + K_{\text{tx}} \frac{N_{\text{tx}}(N_{\text{tx}}+1)}{2} = 4224 + 40 = 4264$  covariance parameters. Since the Kronecker GMM has significantly fewer parameters, it should require a smaller number  $M$  of training data. This is confirmed in Fig. 6 where the two estimators are compared at an SNR of 10 dB for varying  $M$ . The curves intersect between  $M = 10^4$  and  $M = 10^5$ .

### C. Wideband

In this section, we show numerical results for the wideband signal model described in Section II-C and with the QuaDRiGa simulation setup described in Section V-A2. We chose a typical 5G frame structure as defined in [43] with  $N_c = 24$  carriers over a bandwidth of 360 kHz with 15 kHz carrier spacing and with  $N_t = 14$  time symbols over a time slot with 1 ms duration. The number of pilot symbols is  $N_p = 50$ , which means that 50 out of the  $24 \times 14 = 336$  resource elements are occupied with pilot tones. We compare the GMM-based estimator with the LMMSE estimator based on the sample covariance matrix (see (30)), with the CAE approach, and with the ChannelNet estimator (see Section V-B). The training data for each approach consist of  $M = 10^5$  channel realizations and corresponding observations from the pilot positions.

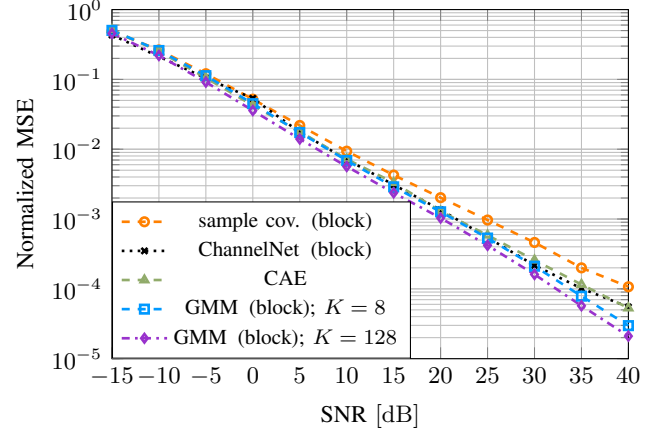


Fig. 7. Wideband signal model (Section II-C) and QuaDRiGa channel model (Section V-A2) with  $N_p = 50$  pilot tones for  $N_c = 24$  carriers and  $N_t = 14$  time symbols for  $v = 3$  km/h.

In Fig. 7, we depict MSE results over the SNR for a scenario where every user moves at  $v = 3$  km/h speed, in which the block-type pilot arrangement has shown the best results. One can observe superior performance of the CAE over the sample covariance LMMSE estimator and the ChannelNet, which may be due to the fact that the CAE optimizes the pilot pattern. However, the GMM approach is able to outperform all baseline algorithms, where the performance gap increases with increasing SNR. Further, the impact of more components (from  $K = 8$  to  $K = 128$ ) is visible and results in better performance for all SNR values.

Fig. 8 shows the same setup but now each user’s velocity is randomly chosen between 0 - 300 km/h (in both training and testing sets), which makes the estimation more challenging and the lattice-type pilot arrangement superior. First, the performance gap to the sample covariance LMMSE estimator increases, which is a result of the more diverse setting that cannot be captured well by a single covariance matrix. Further, the number of GMM components seems to play a more important role. The GMM with  $K = 128$  components is still able to compete with the ChannelNet and CAE approaches.

Finally, Fig. 9 shows the MSE behavior for different numbers of components,  $K$ , and for different amounts of training data used to fit the GMM. Similar to the results in Fig. 4, also the wideband case shows an improving performance for increasing numbers of components. This at least provides numerical evaluation of the convergence of the GMM estimator for noninvertible observation matrices.

## VII. CONCLUSION AND OUTLOOK

We studied the behavior of a GMM channel estimator when the number of GMM components is increased. In case of an invertible observation matrix, we proved the convergence of the GMM estimator to the optimal CME. Notably, the proof only assumes that a sequence of PDFs exists which converges uniformly to the true channel PDF. An example of such a sequence is given by GMMs but no properties unique to GMMs are used in the proof. In particular, any sequence of

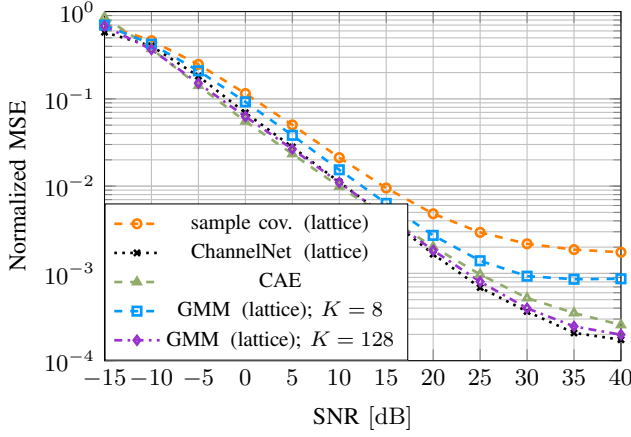


Fig. 8. Wideband signal model (Section II-C) and QuaDRiGa channel model (Section V-A2) with  $N_p = 50$  pilot tones for  $N_c = 24$  carriers and  $N_t = 14$  time symbols for  $v \in [0, 300]$  km/h.

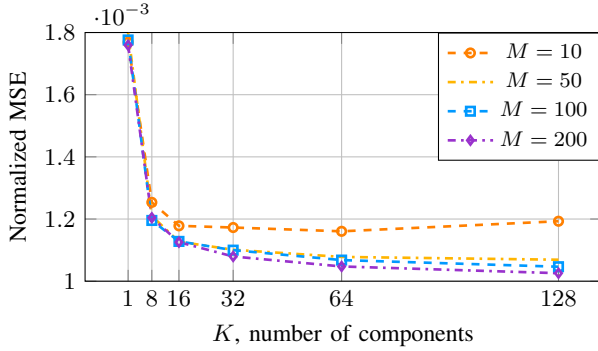


Fig. 9. Wideband signal model (Section II-C) and QuaDRiGa channel model (Section V-A2) with  $N_p = 50$  pilot tones for  $N_c = 24$  carriers and  $N_t = 14$  time symbols for  $v = 3$  km/h and block-type pilot pattern at an SNR of 20 dB. The GMM estimator is trained using  $M \cdot 10^3$  samples.

CMEs which is based on a uniformly convergent sequence of PDFs also converges to the optimal CME. This invites the study of new channel estimators based on other universal approximators.

While the theoretical results are of an asymptotic nature, we analyzed a number of practically relevant settings (SIMO, MIMO, and wideband) in numerical simulations. There, already with a moderate number of GMM components, the proposed estimator outperforms various state-of-the-art approaches in all depicted scenarios. In particular, increasing the number of GMM components lead to a performance improvement even for noninvertible observation matrices. Additionally, we demonstrated how scenario-specific insights can be used to reduce the GMM estimator's complexity.

## APPENDIX A PROOF OF THEOREM 2

The proof of Theorem 2 makes use of and is presented after the following lemma.

**Lemma 1.** For an arbitrary  $\mathbf{y} \in \mathbb{R}^N$ , it holds

$$\int \|\mathbf{h}\| f_n(\mathbf{y} - \mathbf{A}\mathbf{h}) d\mathbf{h} \leq \sqrt{\det(\mathbf{A}^{-1}\mathbf{A}^{-T})} \sqrt{\|\mathbf{A}^{-1}\mathbf{y}\|^2 + \text{trace}(\mathbf{A}^{-1}\mathbf{\Sigma}\mathbf{A}^{-T})}.$$

*Proof.* Recall that  $f_n$  denotes a Gaussian PDF with mean zero and covariance matrix  $\mathbf{\Sigma}$ . We have

$$f_n(\mathbf{y} - \mathbf{A}\mathbf{h}) = \frac{\exp(-\frac{1}{2}(\mathbf{y} - \mathbf{A}\mathbf{h})^T \mathbf{\Sigma}^{-1}(\mathbf{y} - \mathbf{A}\mathbf{h}))}{\sqrt{(2\pi)^N \det(\mathbf{\Sigma})}} \quad (32)$$

$$= \frac{\exp(-\frac{1}{2}(\mathbf{A}^{-1}\mathbf{y} - \mathbf{h})^T \mathbf{A}^T \mathbf{\Sigma}^{-1} \mathbf{A}(\mathbf{A}^{-1}\mathbf{y} - \mathbf{h}))}{\sqrt{(2\pi)^N \det(\mathbf{\Sigma})}} \quad (33)$$

$$= \frac{\exp(-\frac{1}{2}(\mathbf{h} - \mathbf{A}^{-1}\mathbf{y})^T (\mathbf{A}^{-1}\mathbf{\Sigma}\mathbf{A}^{-T})^{-1}(\mathbf{h} - \mathbf{A}^{-1}\mathbf{y}))}{\sqrt{(2\pi)^N \det(\mathbf{\Sigma})}}. \quad (34)$$

Therefore,  $(\sqrt{\det(\mathbf{A}^{-1}\mathbf{A}^{-T})})^{-1} f_n(\mathbf{y} - \mathbf{A}\mathbf{h}) =: \tilde{f}(\mathbf{h})$  is a Gaussian PDF with mean vector  $\tilde{\boldsymbol{\mu}} := \mathbf{A}^{-1}\mathbf{y}$  and covariance matrix  $\tilde{\mathbf{\Sigma}} := \mathbf{A}^{-1}\mathbf{\Sigma}\mathbf{A}^{-T}$ . Let  $\mathbf{w}$  be a standard Gaussian random vector (with mean  $\mathbf{0} \in \mathbb{R}^N$  and covariance matrix  $\mathbf{I} \in \mathbb{R}^{N \times N}$ ) and let  $\tilde{\mathbf{\Sigma}}^{\frac{1}{2}}$  be a square root of the covariance matrix  $\tilde{\mathbf{\Sigma}} = \tilde{\mathbf{\Sigma}}^{\frac{T}{2}} \tilde{\mathbf{\Sigma}}^{\frac{1}{2}}$ . Then, we are interested in computing

$$\int \|\mathbf{h}\| f_n(\mathbf{y} - \mathbf{A}\mathbf{h}) d\mathbf{h} = \sqrt{\det(\mathbf{A}^{-1}\mathbf{A}^{-T})} \int \|\mathbf{h}\| \frac{f_n(\mathbf{y} - \mathbf{A}\mathbf{h})}{\sqrt{\det(\mathbf{A}^{-1}\mathbf{A}^{-T})}} d\mathbf{h} \quad (35)$$

$$= \sqrt{\det(\mathbf{A}^{-1}\mathbf{A}^{-T})} \int \|\mathbf{h}\| \tilde{f}(\mathbf{h}) d\mathbf{h} \quad (36)$$

$$= \sqrt{\det(\mathbf{A}^{-1}\mathbf{A}^{-T})} \mathbb{E}_{\mathbf{w}}[\|\tilde{\boldsymbol{\mu}} + \tilde{\mathbf{\Sigma}}^{\frac{1}{2}}\mathbf{w}\|] \quad (37)$$

where we take the expectation with respect to the standard Gaussian random vector  $\mathbf{w}$ . To see the last equality, note that  $\tilde{\boldsymbol{\mu}} + \tilde{\mathbf{\Sigma}}^{\frac{1}{2}}\mathbf{w}$  is a Gaussian random vector with mean  $\tilde{\boldsymbol{\mu}}$  and covariance matrix  $\tilde{\mathbf{\Sigma}}$ . Jensen's inequality yields:

$$(\mathbb{E}_{\mathbf{w}}[\|\tilde{\boldsymbol{\mu}} + \tilde{\mathbf{\Sigma}}^{\frac{1}{2}}\mathbf{w}\|])^2 \leq \mathbb{E}_{\mathbf{w}}[\|\tilde{\boldsymbol{\mu}} + \tilde{\mathbf{\Sigma}}^{\frac{1}{2}}\mathbf{w}\|^2] \quad (38)$$

$$= \|\tilde{\boldsymbol{\mu}}\|^2 + 2\tilde{\boldsymbol{\mu}}^T \tilde{\mathbf{\Sigma}}^{\frac{1}{2}} \mathbb{E}_{\mathbf{w}}[\mathbf{w}] + \mathbb{E}_{\mathbf{w}}[\text{trace}(\mathbf{w}^T \tilde{\mathbf{\Sigma}}^{\frac{T}{2}} \tilde{\mathbf{\Sigma}}^{\frac{1}{2}} \mathbf{w})] \quad (39)$$

$$= \|\tilde{\boldsymbol{\mu}}\|^2 + \text{trace}(\tilde{\mathbf{\Sigma}} \mathbb{E}_{\mathbf{w}}[\mathbf{w}\mathbf{w}^T]) = \|\tilde{\boldsymbol{\mu}}\|^2 + \text{trace}(\tilde{\mathbf{\Sigma}}) \quad (40)$$

$$= \|\mathbf{A}^{-1}\mathbf{y}\|^2 + \text{trace}(\mathbf{A}^{-1}\mathbf{\Sigma}\mathbf{A}^{-T}). \quad (41)$$

Lastly, we use the square root of this bound in (37).  $\square$

### A. Proof of Theorem 2

First, we show that the convergence of  $f_h^{(K)}$  to  $f_h$  implies the convergence of  $f_y^{(K)}$  to  $f_y$ . The PDF of  $\mathbf{x} := \mathbf{A}\mathbf{h}$  is

$$f_{\mathbf{x}}(\mathbf{x}) = \frac{1}{|\det(\mathbf{A})|} f_h(\mathbf{A}^{-1}\mathbf{x}) \quad (42)$$

because  $\mathbf{A}$  is invertible. Since the random vector  $\mathbf{y} = \mathbf{x} + \mathbf{n}$  is a sum of two stochastically independent random variables, its PDF can be computed via convolution:

$$f_{\mathbf{y}}(\mathbf{y}) = \int f_n(\mathbf{s}) f_{\mathbf{x}}(\mathbf{y} - \mathbf{s}) d\mathbf{s}. \quad (43)$$

Similarly,  $f_y^{(K)}$  is obtained by replacing  $f_x$  with  $f_x^{(K)}$  in (43). For later reference, note that because  $f_n$  is positive ( $f_n(s) > 0$  for all  $s \in \mathbb{R}^N$ ) and  $f_x$  as well as  $f_x^{(K)}$  are continuous PDFs, the convolution results  $f_y^{(K)}$  and  $f_y$  are positive, too. We have

$$|f_y(y) - f_y^{(K)}(y)| \quad (44)$$

$$= \left| \int f_n(s) (f_x(y-s) - f_x^{(K)}(y-s)) ds \right| \quad (45)$$

$$\leq \int \left| f_n(s) \frac{f_h(A^{-1}(y-s)) - f_h^{(K)}(A^{-1}(y-s))}{|\det(A)|} \right| ds \quad (46)$$

$$\leq \frac{\|f_h - f_h^{(K)}\|_\infty}{|\det(A)|} \int |f_n(s)| ds = \frac{\|f_h - f_h^{(K)}\|_\infty}{|\det(A)|}. \quad (47)$$

The last integral is equal to one because  $f_n$  is a PDF. Since  $\lim_{K \rightarrow \infty} \|f_h - f_h^{(K)}\|_\infty = 0$  holds by assumption, we have

$$\lim_{K \rightarrow \infty} \|f_y - f_y^{(K)}\|_\infty = 0. \quad (48)$$

To show (25), let  $y \in \mathcal{B}_r$  be arbitrary. With (7) and (9) in mind, we find the following upper bound:

$$\begin{aligned} \|\hat{h} - \hat{h}^{(K)}\| &\leq \int \|h\| f_n(y - Ah) \left| \frac{f_h(h)}{f_y(y)} - \frac{f_h^{(K)}(h)}{f_y^{(K)}(y)} \right| dh \\ &\leq \sup_{h \in \mathbb{R}^N} \left| \frac{f_h(h)}{f_y(y)} - \frac{f_h^{(K)}(h)}{f_y^{(K)}(y)} \right| \int \|h\| f_n(y - Ah) dh. \end{aligned} \quad (49)$$

The last integral is independent of  $K$  and by Lemma 1, it is finite for any  $y \in \mathbb{R}^N$ . It is in particular bounded by

$$\sqrt{\det(A^{-1}A^{-T})} \sqrt{\|A^{-1}\|^{2r^2} + \text{trace}(A^{-1}\Sigma A^{-T})} < \infty$$

for all  $y \in \mathcal{B}_r$ . Hence, as soon as

$$\lim_{K \rightarrow \infty} \sup_{h \in \mathbb{R}^N} \left| \frac{f_h(h)}{f_y(y)} - \frac{f_h^{(K)}(h)}{f_y^{(K)}(y)} \right| = 0, \quad \forall y \in \mathcal{B}_r \quad (50)$$

is shown, (25) is confirmed.

To prove (50), we write

$$\left| \frac{f_h(h)}{f_y(y)} - \frac{f_h^{(K)}(h)}{f_y^{(K)}(y)} \right| = \left| \frac{f_h(h)f_y^{(K)}(y) - f_y(y)f_h^{(K)}(h)}{f_y(y)f_y^{(K)}(y)} \right| \quad (51)$$

for an arbitrary  $h \in \mathbb{R}^N$ . Now, we add  $0 = f_y^{(K)}(y)f_h^{(K)}(h) - f_y^{(K)}(y)f_h^{(K)}(h)$  in the numerator on the right-hand side and apply the triangle inequality to get

$$\left| \frac{f_h(h)f_y^{(K)}(y) - f_y(y)f_h^{(K)}(h)}{f_y(y)f_y^{(K)}(y)} \right| \quad (52)$$

$$\leq \frac{\left| (f_h(h) - f_h^{(K)}(h)) f_y^{(K)}(y) \right|}{f_y(y)f_y^{(K)}(y)} + \frac{\left| (f_y^{(K)}(y) - f_y(y)) f_h^{(K)}(h) \right|}{f_y(y)f_y^{(K)}(y)} \quad (53)$$

$$\leq \frac{\|f_h - f_h^{(K)}\|_\infty \|f_y^{(K)}\|_\infty + \|f_y^{(K)} - f_y\|_\infty \|f_h^{(K)}\|_\infty}{f_y(y)f_y^{(K)}(y)}. \quad (54)$$

By compactness of  $\mathcal{B}_r$  and continuity of  $f_y$ , there exists a  $y_{\min} \in \mathcal{B}_r$  at which  $f_y$  attains a minimum value  $f_y(y_{\min}) > 0$  over  $\mathcal{B}_r$ . Due to the uniform convergence (48), there exists an index  $N_1 \in \mathbb{N}$  such that  $|f_y(y) - f_y^{(K)}(y)| \leq \frac{1}{2} f_y(y_{\min})$  holds for all  $K \geq N_1$  and for all  $y \in \mathcal{B}_r$ . The reverse triangle inequality then shows that  $f_y^{(K)}(y) \geq f_y(y) - |f_y(y) - f_y^{(K)}(y)| \geq f_y(y_{\min}) - \frac{1}{2} f_y(y_{\min}) = \frac{1}{2} f_y(y_{\min})$  is true. Hence, with  $M_1 := \frac{1}{2} f_y(y_{\min}) > 0$ , the inequality

$$f_y^{(K)}(y) \geq M_1 \quad (55)$$

holds for all  $y \in \mathcal{B}_r$  and for all  $K \geq N_1$ . Further, since  $\|f_h - f_h^{(K)}\|_\infty \rightarrow 0$  and  $\|f_h\|_\infty < \infty$ , there exist  $M_2 > 0$  and  $N_2 \in \mathbb{N}$  such that

$$\|f_h^{(K)}\|_\infty \leq M_2 \quad \text{for all } K \geq N_2. \quad (56)$$

Analogously, there exist  $M_3 > 0$  and  $N_3 \in \mathbb{N}$  such that

$$\|f_y^{(K)}\|_\infty \leq M_3 \quad \text{for all } K \geq N_3. \quad (57)$$

Let  $\varepsilon > 0$  be arbitrary. Due to  $\|f_h - f_h^{(K)}\|_\infty \rightarrow 0$ , there exists an index  $N_4 \geq \max\{N_1, N_3\}$  such that

$$\|f_h - f_h^{(K)}\|_\infty \leq \frac{f_y(y_{\min})M_1}{2M_3} \varepsilon \quad \text{for all } K \geq N_4. \quad (58)$$

Similarly, there exists an index  $N_5 \geq \max\{N_1, N_2\}$  with

$$\|f_y - f_y^{(K)}\|_\infty \leq \frac{f_y(y_{\min})M_1}{2M_2} \varepsilon \quad \text{for all } K \geq N_5. \quad (59)$$

We can use the last five inequalities to bound (54). To this end,  $f_y(y_{\min})$  and (55) provide bounds on the terms in the denominator, (58) and (57) bound the first summand in the numerator, and (59) and (56) bound the second summand in the numerator. In total, this yields an upper bound on (51):

$$\begin{aligned} \left| \frac{f_h(h)}{f_y(y)} - \frac{f_h^{(K)}(h)}{f_y^{(K)}(y)} \right| &\leq \frac{f_y(y_{\min})M_1}{2M_3} \varepsilon \cdot \frac{M_3}{f_y(y_{\min})M_1} \\ &\quad + \frac{f_y(y_{\min})M_1}{2M_2} \varepsilon \cdot \frac{M_2}{f_y(y_{\min})M_1}. \end{aligned} \quad (60)$$

for all  $K \geq \max\{N_4, N_5\}$  and for all  $y \in \mathcal{B}_r$ . We conclude

$$\sup_{h \in \mathbb{R}^N} \left| \frac{f_h(h)}{f_y(y)} - \frac{f_h^{(K)}(h)}{f_y^{(K)}(y)} \right| \leq \varepsilon \quad (61)$$

for all  $K \geq \max\{N_4, N_5\}$  and all  $y \in \mathcal{B}_r$ , and because  $\varepsilon$  was arbitrary, (50) is confirmed, which finishes the proof.

## APPENDIX B

### INTEGRAL FOR NONINVERTIBLE MATRICES

To see why  $\int \|h\| f_n(y - Ah) dh$  might not be finite, consider the matrix  $A = [I, 0] \in \mathbb{R}^{m \times N}$  where  $I \in \mathbb{R}^{m \times m}$  is the identity matrix and the remaining matrix elements are zero. Let us write  $h = [h_m^T, h_{N-m}^T]^T \in \mathbb{R}^m \times \mathbb{R}^{N-m}$ . Define the set  $\mathcal{C} = \{h \in \mathbb{R}^N \mid \|h_m\| \geq 1, \|h_{N-m}\| \geq 1\}$  where the norm of both sub-vectors  $h_m$  and  $h_{N-m}$  is at least one such that we always have  $\|h\| \geq 1$  on  $\mathcal{C}$ . We can now compute:

$$\int_{\mathbb{R}^N} \|h\| f_n(y - Ah) dh \geq \int_{\mathcal{C}} f_n(y - Ah) dh \quad (62)$$

$$= \int_{\|h_{N-m}\| \geq 1} \int_{\|h_m\| \geq 1} f_n(y - h_m) dh_m dh_{N-m}. \quad (63)$$

Since  $f_n$  is an  $m$ -dimensional Gaussian PDF, the inner integral is equal to some constant  $c$  with  $0 < c < 1$  and it follows that  $\int \|\mathbf{h}\| f_n(\mathbf{y} - \mathbf{A}\mathbf{h}) d\mathbf{h}$  is not finite.

## APPENDIX C ON THE UNIFORM CONVERGENCE

Let us express the PDF of  $\mathbf{A}\mathbf{h}$ . If  $\mathbf{A} \in \mathbb{R}^{m \times N}$  is a wide matrix with full rank  $m$ , we can assume that the first  $m$  columns are linearly independent (otherwise we introduce a permutation matrix). This allows us to partition  $\mathbf{A} = [\mathbf{A}_i, \mathbf{A}_n]$  into an invertible part  $\mathbf{A}_i \in \mathbb{R}^{m \times m}$  and a noninvertible part  $\mathbf{A}_n \in \mathbb{R}^{m \times N-m}$ . With a corresponding partitioning of  $\mathbf{h} = [\mathbf{h}_i^T, \mathbf{h}_n^T]^T \in \mathbb{R}^m \times \mathbb{R}^{N-m}$ , we have  $\mathbf{x} = \mathbf{A}\mathbf{h} = \mathbf{A}_i\mathbf{h}_i + \mathbf{A}_n\mathbf{h}_n$  and we can define an invertible mapping  $t : \mathbb{R}^N \rightarrow \mathcal{X} \times \mathcal{X}'$ :

$$t : (\mathbf{h}_i, \mathbf{h}_n) \mapsto (\mathbf{A}_i\mathbf{h}_i + \mathbf{A}_n\mathbf{h}_n, \mathbf{h}_n) = (\mathbf{x}, \mathbf{x}') \quad (64)$$

$$t^{-1} : (\mathbf{x}, \mathbf{x}') \mapsto (\mathbf{A}_i^{-1}(\mathbf{x} - \mathbf{A}_n\mathbf{x}'), \mathbf{x}') = (\mathbf{h}_i, \mathbf{h}_n) \quad (65)$$

with  $\mathcal{X} \subseteq \mathbb{R}^m$ ,  $\mathcal{X}' \subseteq \mathbb{R}^{N-m}$ . We can now compute the joint density  $f_{\mathbf{x}, \mathbf{x}'}$  with the usual transformation formula:

$$f_{\mathbf{x}, \mathbf{x}'}(\mathbf{x}, \mathbf{x}') = \begin{cases} \frac{f_{\mathbf{h}}(t^{-1}(\mathbf{x}, \mathbf{x}'))}{|\det(\frac{\partial t}{\partial \mathbf{h}}(g^{-1}(\mathbf{x}, \mathbf{x}')))|}, & \text{if } (\mathbf{x}, \mathbf{x}') \in \mathcal{X} \times \mathcal{X}' \\ 0, & \text{if } (\mathbf{x}, \mathbf{x}') \notin \mathcal{X} \times \mathcal{X}'. \end{cases} \quad (66)$$

Together with  $|\det(\frac{\partial t}{\partial \mathbf{h}}(t^{-1}(\mathbf{x}, \mathbf{x}')))| = |\det(\mathbf{A}_i)|$ , we can express the PDF of  $\mathbf{x} = \mathbf{A}\mathbf{h}$  via marginalization:

$$f_{\mathbf{x}}(\mathbf{x}) = \int_{\mathcal{X}'} f_{\mathbf{x}, \mathbf{x}'}(\mathbf{x}, \mathbf{x}') d\mathbf{x}' = \int_{\mathcal{X}'} \frac{f_{\mathbf{h}}(t^{-1}(\mathbf{x}, \mathbf{x}'))}{|\det(\mathbf{A}_i)|} d\mathbf{x}'. \quad (67)$$

Analogously, one obtains  $f_{\mathbf{x}}^{(K)}$  for  $\mathbf{x}^{(K)} = \mathbf{A}\mathbf{h}^{(K)}$ . Given

$$|f_{\mathbf{x}}^{(K)}(\mathbf{x}) - f_{\mathbf{x}}(\mathbf{x})| = \frac{1}{|\det(\mathbf{A}_i)|} \times \left| \int_{\mathcal{X}'} \left( f_{\mathbf{h}}^{(K)}(t^{-1}(\mathbf{x}, \mathbf{x}')) - f_{\mathbf{h}}(t^{-1}(\mathbf{x}, \mathbf{x}')) \right) d\mathbf{x}' \right|, \quad (68)$$

we can conjecture that due to the integral over  $\mathcal{X}'$  the uniform convergence of  $f_{\mathbf{h}}^{(K)}$  to  $f_{\mathbf{h}}$  alone is generally not sufficient to infer the uniform convergence of  $f_{\mathbf{x}}^{(K)}$  to  $f_{\mathbf{x}}$ .

## REFERENCES

- [1] M. Koller, B. Fesl, N. Turan, and W. Utschick, "An asymptotically optimal approximation of the conditional mean channel estimator based on Gaussian mixture models," *CoRR*, vol. abs/2111.11064, 2021. [Online]. Available: <https://arxiv.org/abs/2111.11064>
- [2] F. Rusek, D. Persson, B. K. Lau, E. G. Larsson, T. L. Marzetta, O. Edfors, and F. Tufvesson, "Scaling up MIMO: Opportunities and challenges with very large arrays," *IEEE Signal Process. Mag.*, vol. 30, no. 1, pp. 40–60, Jan. 2013.
- [3] D. C. Araújo, A. L. F. de Almeida, J. Axnäs, and J. C. M. Mota, "Channel estimation for millimeter-wave very-large MIMO systems," in *2014 22nd Eur. Signal Process. Conf. (EUSIPCO)*, Sep. 2014, pp. 81–85.
- [4] M. K. Samimi and T. S. Rappaport, "3-D millimeter-wave statistical channel model for 5G wireless system design," *IEEE Trans. Microw. Theory Techn.*, vol. 64, no. 7, pp. 2207–2225, Jul. 2016.
- [5] 3GPP, "Spatial channel model for multiple input multiple output (MIMO) simulations," 3rd Generation Partnership Project (3GPP), Tech. Rep. 25.996 (V16.0.0), Jul. 2020.
- [6] S. Jaeckel, L. Raschkowski, K. Börner, and L. Thiele, "QuaDRiGa: A 3-D multi-cell channel model with time evolution for enabling virtual field trials," *IEEE Trans. Antennas Propag.*, vol. 62, no. 6, pp. 3242–3256, 2014.
- [7] S. Jaeckel, L. Raschkowski, K. Börner, L. Thiele, F. Burkhardt, and E. Eberlein, "QuaDRiGa: Quasi deterministic radio channel generator, user manual and documentation," Fraunhofer Heinrich Hertz Institute, Tech. Rep., v2.2.0, 2019.
- [8] A. Alkhateeb, "DeepMIMO: A generic deep learning dataset for millimeter wave and massive MIMO applications," in *Proc. of Inf. Theory and Appl. Workshop (ITA)*, San Diego, CA, Feb. 2019, pp. 1–8.
- [9] T. T. Nguyen, H. D. Nguyen, F. Chamroukhi, and G. J. McLachlan, "Approximation by finite mixtures of continuous density functions that vanish at infinity," *Cogent Math. Statist.*, vol. 7, no. 1, p. 1750861, 2020.
- [10] Y. Gu and Y. D. Zhang, "Information-theoretic pilot design for downlink channel estimation in FDD massive MIMO systems," *IEEE Trans. Signal Process.*, vol. 67, no. 9, pp. 2334–2346, May 2019.
- [11] S. Coleri, M. Ergen, A. Puri, and A. Bahai, "Channel estimation techniques based on pilot arrangement in OFDM systems," *IEEE Trans. Broadcast.*, vol. 48, no. 3, pp. 223–229, 2002.
- [12] C. M. Bishop, *Pattern Recognition and Machine Learning (Information Science and Statistics)*. Berlin, Heidelberg: Springer-Verlag, 2006.
- [13] J. P. Vila and P. Schniter, "Expectation-maximization Gaussian-mixture approximate message passing," *IEEE Trans. Signal Process.*, vol. 61, no. 19, pp. 4658–4672, Oct. 2013.
- [14] C.-K. Wen, S. Jin, K.-K. Wong, J.-C. Chen, and P. Ting, "Channel estimation for massive MIMO using Gaussian-mixture Bayesian learning," *IEEE Trans. Wireless Commun.*, vol. 14, no. 3, pp. 1356–1368, Mar. 2015.
- [15] P. Su and Y. Wang, "Channel estimation in massive MIMO systems using a modified Bayes-GMM method," *Wireless Personal Communications*, vol. 107, Aug. 2019.
- [16] X. Wei, C. Hu, and L. Dai, "Deep learning for beamspace channel estimation in millimeter-wave massive MIMO systems," *IEEE Trans. Commun.*, vol. 69, no. 1, pp. 182–193, Jan. 2021.
- [17] P. Mukherjee, D. Mishra, and S. De, "Gaussian mixture based context-aware short-term characterization of wireless channels," *IEEE Trans. Veh. Technol.*, vol. 69, no. 1, pp. 26–40, Jan. 2020.
- [18] H. Zhang, J. Xue, D. Meng, Q. Zhao, and Z. Xu, "Robust CSI estimation under complex communication environment," in *ICC 2019 - 2019 IEEE International Conference on Communications (ICC)*, May 2019, pp. 1–6.
- [19] E. Nayeibi and B. D. Rao, "Semi-blind channel estimation in massive MIMO systems with different priors on data symbols," in *2018 IEEE International Conference on Acoustics, Speech and Signal Processing (ICASSP)*, Apr. 2018, pp. 3879–3883.
- [20] Y. Li, J. Zhang, Z. Ma, and Y. Zhang, "Clustering analysis in the wireless propagation channel with a variational Gaussian mixture model," *IEEE Trans. Big Data*, vol. 6, no. 2, pp. 223–232, Jun. 2020.
- [21] Y. Li, J. Zhang, P. Tang, and L. Tian, "Clustering in the wireless channel with a power weighted statistical mixture model in indoor scenario," *China Commun.*, vol. 16, no. 7, pp. 83–95, Jul. 2019.
- [22] S. Jiang, X. Yuan, X. Wang, C. Xu, and W. Yu, "Joint user identification, channel estimation, and signal detection for grant-free NOMA," *IEEE Trans. Wireless Commun.*, vol. 19, no. 10, pp. 6960–6976, Oct. 2020.
- [23] Y. Gu and Y. D. Zhang, "Pilot design for Gaussian mixture channel estimation in massive MIMO," in *2018 IEEE Int. Conf. Acoustics, Speech and Signal Process. (ICASSP)*, Apr. 2018, pp. 3266–3270.
- [24] G. Schay, *Introduction to Probability with Statistical Applications*. Birkhäuser Boston, Jun. 2016.
- [25] R. M. Gray, "Toeplitz and circulant matrices: A review," *Foundations and Trends® in Communications and Information Theory*, no. 3, pp. 155–239, 2006.
- [26] J. Kermaol, L. Schumacher, K. Pedersen, P. Mogensen, and F. Frederiksen, "A stochastic MIMO radio channel model with experimental validation," *IEEE J. Sel. Areas Commun.*, vol. 20, no. 6, pp. 1211–1226, 2002.
- [27] M. Šimko, C. Mehlhöfer, M. Wulrich, and M. Rupp, "Doubly dispersive channel estimation with scalable complexity," in *2010 International ITG Workshop on Smart Antennas (WSA)*, Feb. 2010, pp. 251–256.
- [28] S. Resnick, *A Probability Path*, ser. Modern Birkhäuser Classics. Birkhäuser Boston, 2005.
- [29] A. Klenke, *Probability Theory: A Comprehensive Course*. Springer, 2008.
- [30] E. M. Goggin, "Convergence in distribution of conditional expectations," *The Annals of Probability*, vol. 22, no. 2, pp. 1097–1114, 1994.
- [31] D. Neumann, T. Wiese, and W. Utschick, "Learning the MMSE channel estimator," *IEEE Trans. Signal Process.*, vol. 66, no. 11, pp. 2905–2917, Jun. 2018.
- [32] M. Kurras, S. Dai, S. Jaeckel, and L. Thiele, "Evaluation of the spatial consistency feature in the 3GPP geometry-based stochastic channel

- model,” in *2019 IEEE Wireless Communications and Networking Conference (WCNC)*, Apr. 2019, pp. 1–6.
- [33] A. Alkhateeb, G. Leus, and R. W. Heath, “Compressed sensing based multi-user millimeter wave systems: How many measurements are needed?” in *2015 IEEE Int. Conf. Acoustics, Speech and Signal Process. (ICASSP)*, 2015, pp. 2909–2913.
  - [34] G. Davis, S. Mallat, and M. Avellaneda, “Adaptive greedy approximations,” *Constructive Approximation*, vol. 13, no. 1, pp. 57–98, Mar. 1997.
  - [35] Y. C. Pati, R. Rezaeiifar, and P. S. Krishnaprasad, “Orthogonal matching pursuit: Recursive function approximation with applications to wavelet decomposition,” in *Proc. 27th Asilomar Conf. Signals, Systems, and Computers*, Nov. 1993, pp. 40–44 vol.1, ISSN: 1058-6393.
  - [36] J. A. Tropp, “Greed is good: Algorithmic results for sparse approximation,” *IEEE Trans. Inf. Theory*, vol. 50, no. 10, pp. 2231–2242, Oct. 2004.
  - [37] D. L. Donoho, A. Maleki, and A. Montanari, “Message passing algorithms for compressed sensing: I. motivation and construction,” in *2010 IEEE Inf. Theory Workshop on Inf. Theory (ITW 2010, Cairo)*, Jan. 2010, pp. 1–5.
  - [38] A. Maleki, L. Anitori, Z. Yang, and R. G. Baraniuk, “Asymptotic analysis of complex LASSO via complex approximate message passing (CAMP),” *IEEE Trans. Inf. Theory*, vol. 59, no. 7, pp. 4290–4308, Jul. 2013.
  - [39] B. Fesl, N. Turan, M. Koller, and W. Utschick, “A low-complexity MIMO channel estimator with implicit structure of a convolutional neural network,” in *2021 IEEE 22nd Int. Workshop on Signal Process. Adv. in Wireless Commun. (SPAWC)*, 2021, accepted, arXiv preprint: 2104.12667.
  - [40] M. F. Balin, A. Abid, and J. Zou, “Concrete autoencoders: Differentiable feature selection and reconstruction,” in *Proceedings of the 36th International Conference on Machine Learning*, vol. 97. PMLR, Jun. 2019, pp. 444–453.
  - [41] M. Soltani, V. Pourahmadi, and H. Sheikhzadeh, “Pilot pattern design for deep learning-based channel estimation in OFDM systems,” *IEEE Wireless Commun. Lett.*, vol. 9, no. 12, pp. 2173–2176, 2020.
  - [42] M. Soltani, V. Pourahmadi, A. Mirzaei, and H. Sheikhzadeh, “Deep learning-based channel estimation,” *IEEE Commun. Lett.*, vol. 23, no. 4, pp. 652–655, 2019.
  - [43] 3GPP, “NR; Physical channels and modulation,” 3rd Generation Partnership Project (3GPP), Tech. Spec. 38.211 (V16.7.0), Sep. 2021.